Numerical study of optical ray retracing in laser-plasma backscatter

R. H. Lehmberg and K. A. Holder
Naval Research Laboratory, Washington, D.C. 20375
(Received 22 January 1980)

Optical ray retracing in stimulated Brillouin backscatter from laser-produced plasmas is studied numerically, using a 2-D propagation code (BOUNCE). This code treats steady-state behavior in the strong damping limit, and includes self-focusing effects. Ray retracing phenomena are grouped into two limiting cases. In the "whole-beam" limit, the pump field at the lens has a broad spatial profile that can be focused to a long narrow waist within the plasma. This geometry selectively amplifies only those initial noise components that are propagating back along the axis, where the net gain is highest. The simulations show that such effects exhibit a pronounced threshold due to self-focusing, and disappear when the focal width becomes comparable to the length of the gain medium. In the opposite limit, where the pump radiation at the lens is dominated by small-scale transverse structure, the backscatter can reproduce this structure in detail (i.e., exhibit wavefront reversal) when the far field of the pump produces an interference pattern in the plasma. The plasma then behaves as an active volume hologram as it amplifies the backward-propagating random noise fields. If the target is moved far out of focus so that the pump components can no longer interfere, the ray retracing disappears, and the actual backscatter profile depends upon the noise structure. Wavefront reversal is found to be influenced by several other factors, including focal spot size, spatial gain narrowing, gain inhomogeneity, and self-focusing. The simulations show that it is most pronounced when the spatial profiles of the pump and the backscatter are wide in comparison to the transverse wavelengths of the interference structure, and the $1/e$ gain length (especially in the last one or two e foldings) is large in comparison to the optical diffraction lengths. It is enhanced significantly if the plasma has a monotonically decreasing gain coefficient away from the target. In the strong-damping limit, where the nonlinear phase change/cm is comparable to the gain coefficient, filamentation can be important near the target; however, its effect on small-scale ray retracing is usually minimal, provided that the above conditions are satisfied. If the focal spot decreases below a critical width, however, whole-beam self-focusing takes over and quickly destroys the small-scale retrace.

I. INTRODUCTION

Optical ray retracing, in which the transverse spatial pattern of an incident beam is reproduced by its backscatter, is a well-known feature of stimulated Brillouin scattering. The effect has been studied in liquids[1-4] and extended plasmas,[5,6] as well as in laser-produced plasmas.[7-10] In the latter case, it occurs even when the critical surface is oriented to produce a strong off-axis specular reflection, as shown by the experiment illustrated in Fig. 1.[10] This paper describes numerical simulations of ray retracing in laser-produced plasmas, using a steady-state 2D propagation code (BOUNCE).[11] In its present form, the code treats steady-state behavior in the strong (ion-acoustic) damping limit,[12,13] and includes self-focusing due to the pondermotive force[14]; however, it ignores pump depletion, self-consistent ion heating,[12] and ion wave saturation effects.[5,15-17]

It is useful to classify ray retrace phenomena roughly into two limiting cases. In the "whole beam" case, the pump field incident at the lens has a broad smoothly varying spatial profile (e.g., Gaussian or hyper-Gaussian) that can be focused to a long narrow waist within the plasma. The narrow waist selectively amplifies only those components of the incident noise spectrum that are propagating back along the near-axial directions, where the net gain is highest. The simulations show that the ray retracing associated with this effect can exhibit a pronounced threshold due to self-focusing, and disappears when the focal width becomes comparable to the length of the gain medium. They also show that although the angular distribution of the backscatter at the lens is qualitatively similar to that of the pump, it will usually be somewhat broader. This arises from spatial gain narrowing[18] of the backscatter profile within the plasma, which leads to a greater diffraction

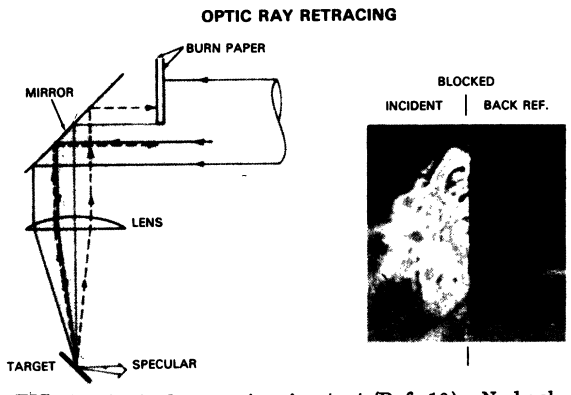

FIG. 1. Optical ray retracing test (Ref. 10). No back-reflection exposure is found on the blocked half of the beam, indicating that ray retracing occurs.

spreading as the radiation returns to the lens.

In the opposite limit, where the pump field is dominated by small-scale transverse inhomogeneity, the backscatter can reproduce this structure in detail under certain conditions. An example of this is the well-known "question mark" experiment performed by Eidmann and Sigel,[7] in which the Brillouin backscattered from a laser-produced plasma retraces an intensity pattern imposed on the pump beam by an apertured mask near the focusing lens. The phenomenon has also been observed in the Brillouin[4] and Raman[19] backscatter from liquids. Ray retracing behavior in which the spatial structure at the lens resides entirely in the phase rather than the irradiance has been studied extensively,[1,2,20] and the feasibility of using this effect to correct phase aberrations in a laser system has been demonstrated.[3]

In ideal cases, small-scale ray retracing can be described as wavefront reversal (or phase conjugation), in which the backscatter amplitude $\mathcal{E}_1(\vec{r})$ is proportional to the conjugate amplitude $\mathcal{E}_0^*(\vec{r})$ of the incident radiation.[1] Theoretical studies of Zel'dovich and others[1,21-23] indicate that phase conjugation occurs under conditions where any small fraction of the initial noise field that happens to be proportional to $\mathcal{E}_0^*(\vec{r})$ can grow faster than the remaining portions, and thus eventually predominates. The physical basis for wavefront reversal can be readily visualized in the case where the pump profile at the lens consists of two or more isolated hot spots. The beams from these hot spots overlap near focus to create an interference pattern in the plasma. This pattern selectively amplifies only those noise components propagating opposite to any one of the pump beams, and simultaneously Bragg-diffracts energy back along all of the remaining beams.[11,24-26] If the plasma is moved far out of focus, so that the beams no longer overlap, then the wavefront reversal disappears, and the actual backscatter profile depends upon the incident noise structure.

To examine this mechanism in greater detail, consider the simple model shown in Fig. 2. A pair of isolated pump beams with propagation vectors $\vec{k}_0$ and $\vec{k}_0'$, and initial widths Δ_B are focused into a plasma slab of thickness $L \gg \lambda_0$. In the focal region, the beam waists (indicated by the dashed lines) overlap to produce an interference pattern $|\mathcal{E}_0(\vec{r})|^2$ of spatial frequency $\vec{K} \equiv \vec{k}_0' - \vec{k}_0$, width $d \simeq 2\lambda_0 f/\Delta_B \gg \lambda_0$, and length $8\lambda_0 f^2/\Delta_B^2 > L$, where f is the focal length of the lens. A plane-wave noise field incident along some backward direction $\vec{k}_1$ therefore sees a periodic gain coefficient proportional to $|\mathcal{E}_0(\vec{r})|^2$, as indicated by the parallel lines in Fig. 2. If the dimensions L and d are large in comparison to the periodicity $\Lambda = 2\pi/K$,

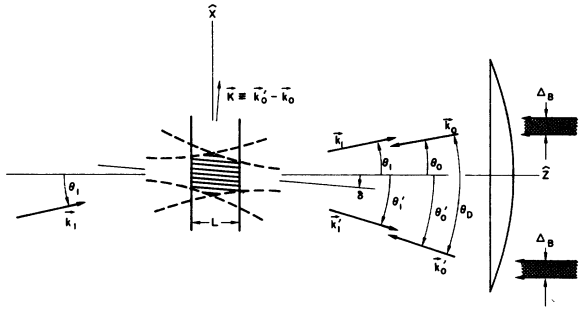

FIG. 2. Bragg diffraction of a backward propagating noise wave $\vec{k}_1$ in the active volume hologram created by two interfering pump waves, $\vec{k}_0$ and $\vec{k}_0'$, in a Brillouin-active medium. Note that the angles θ_0', θ_1', and δ are negative in this illustration.

then the region behaves as an active volume hologram.[27] The $\vec{k}_1$ wave will grow most rapidly, while simultaneously Bragg-diffracting energy into the $\vec{k}_1'$ mode, when this pair of coupled waves satisfies the Bragg condition

$$\vec{k}_1 - \vec{k}_1' = \vec{k}_0' - \vec{k}_0 = \vec{K} \tag{1}$$

within the medium.[28] The gain is maximum when the periodic intensity pattern $|\mathcal{E}_1(\vec{r})|^2$ developed by the $\vec{k}_1, \vec{k}_1'$ waves is exactly in phase with that of $|\mathcal{E}_0(\vec{r})|^2$; i.e., when $\vec{k}_1 = -\vec{k}_0$ and $\vec{k}_1' = -\vec{k}_0'$. Since $k_1' = k_1 \simeq k_0$ for Brillouin scattering, this condition occurs when $\theta_1 \simeq \theta_0$ and $\theta_1' \simeq \theta_0'$. Any arbitrary phase difference ϕ between the pump beams will also be reproduced in the two backscattered beams [i.e., $\mathcal{E}_1(\vec{r}) \sim \mathcal{E}_0^*(\vec{r})$] because the backscatter phase difference depends upon the phase of the interference pattern, which in turn depends upon ϕ.

A coupled wave analysis[11,24] has shown that the intensities of the two backscattered beams become nearly equal after a few e foldings, and that the gain maximizes at $\theta_1 = \theta_0$ (assuming $k_1 = k_0$) with a $1/e$ angular bandpass $\delta\theta_1 \sim 1/k_0\theta_D$. ($\theta_D$ is defined in Fig. 2). For a uniform medium of thickness L and average amplitude gain coefficient $\alpha \gg L^{-1}$, one obtains $\delta\theta_1 = (8/\alpha L)^{1/2}\alpha/k_0\theta_D$, giving an angular resolution ($\theta_D \to \delta\theta_1$)

$$(\theta_D)_{\min} = (8/\alpha L)^{1/4}(\alpha/k_0)^{1/2}. \tag{2a}$$

For a semi-infinite medium of exponentially decreasing gain $\alpha(z) = \alpha_0 \exp(-z/l)$, where $\alpha_0 l \gg 1$, one obtains

$$(\theta_D)_{\min} = (2.32/k_0 l)^{1/2}. \tag{2b}$$

As long as the widths of the focal spot and backscatter remain large in comparison to the transverse period Λ, the wave-front reversal will be evident if $\theta_D \gg (\theta_D)_{\min}$. For a fixed gain, Eq. (2a) requires that the diffraction length $1/k_0\theta_D^2$ must be much shorter than the effective gain length $1/\alpha$,[21,22] or in terms of the spatial frequency $\vec{K}$ of the in-

terference pattern,

$$K^2/k_0 \gg \alpha . \tag{3}$$

The physical argument for this requirement can be stated as follows: As long as there is enough gain, the transverse intensity variation of the pump will *always* tend to "pull" the backscatter intensity into a similar pattern as it propagates back through the active medium.[22] However, if this pulling effect occurs in too short a distance, the backscatter phase (which cannot be directly effected) will remain similar to that of the incident noise, which is uncorrelated with the pump phase. The backscatter would then begin to diverge from the pump as soon as it leaves the active medium. (Within the context of the above model, the medium would behave as a simple diffraction grating with many orders, rather than a volume hologram.) Now consider the case where the gain occurs slowly in comparison to diffraction. The amplification then takes place over a long path that effectively filters out all of the backward propagating modes excepting the one that would have developed the transverse intensity pattern even without the pulling effect; i.e., the mode proportional to $\mathcal{E}_0^*(\vec{r})$.

The numerical calculations presented here will illustrate the main results of the volume hologram model, and explore the influence of several factors (e.g., focal spot size, spatial gain narrowing,[11,18,29] longitudinal gain inhomogeneity, and filamentation) on the small-scale ray retracing. The simulations show that small-scale retracing is most pronounced when (i) the power gain is >1000, (ii) the focal spot and backscatter remain wide in comparison to the period of the transverse interference structure, and (iii) the $1/e$ gain length (especially in the last one or two e foldings) is large in comparison to the diffraction length of the interference structure. It is enhanced, for example, if the plasma has a monotonically decreasing density (and therefore gain coefficient) away from the target.[10] In the strong-damping limit, where the nonlinear phase change/cm is comparable to the gain coefficient,[30] filamentation can be important near the target[14,31]; however, its effect on small-scale ray retracing is usually minimial (with the density gradient) if the above conditions are satisfied. If the focal spot decreases below a critical width, however, whole beam self-focusing takes over and quickly destroys the small-scale retrace.

In the following section, the reduced wave equations are derived for the steady-state pump and backscatter amplitudes in the strongly damped limit, assuming paraxial ray conditions. Section III describes the propagation code, and compares it to an analytic calculation for a simple test problem. Section IV presents numerical simulations with 1.06 μm radiation for several cases, including both whole-beam and small-scale retrace effects. These results are summarized in Sec. V.

II. THEORY

Stimulated Brillouin scattering arises from the interaction between a pair of optical waves $E_0(\vec{r},t), E_1(\vec{r},t)$ of frequencies $\omega_0 \simeq \omega_1$ and an ion-acoustic density fluctuation $\delta n(\vec{r},t)$ of frequency $\omega_0 - \omega_1$. This interaction can be described by Maxwell's equations and the two-fluid plasma equations (neglecting electron inertia) with an oscillating pondermotive force.[17,32,33] Similarly, intensity-dependent variations of the time-averaged plasma density $n(\vec{r})$ can be related to the quasistatic pondermotive pressure.[14] For $|\delta n(\vec{r},t)| \ll n(\vec{r})$, the results are

$$\left(\frac{\partial^2}{\partial t^2} + \frac{4\pi e^2}{m}\, n - c^2\vec{\nabla}^2\right) E_{0,1} = -\frac{4\pi e^2}{m}\,\delta n E_{1,0}\,, \tag{4a}$$

$$\left(\frac{\partial^2}{\partial t^2} + \Delta\omega_s \frac{\partial}{\partial t} - c_s^2\vec{\nabla}^2\right)\delta n = \frac{Ze^2}{2Mm\omega_0\omega_1}\vec{\nabla}\cdot\left[\delta n\vec{\nabla}(E_0^2 + E_1^2)_{\rm av} + 2n\vec{\nabla}(E_0E_1)\right], \tag{4b}$$

where $\Delta\omega_s$ is the acoustic energy damping rate,

$$c_s = [(ZT_e + 3T_i)/M]^{1/2} \tag{5}$$

is the acoustic propagation velocity, Z is the ion charge, $m(M)$ is the electron (ion) mass, $T_e(T_i)$ is the electron (ion) temperature, and $(\,)_{\rm av}$ denotes a time average over one optical cycle. The first two terms on the right-hand side, which arise from the quasi-static pondermotive forces, are usually ignored in 1D treatments, where the spatial variation of the pump intensity is sufficiently weak. If the acoustic transit time across the focal spot is short in comparison to the pulsewidth, then $n(\vec{r})$ is determined by the quasi-static pressure balance[14]:

$$\nabla[(T_e + T_i/Z)n] + (n/8\pi n_c)\nabla(E_0^2 + E_1^2)_{\rm av} = 0\,, \tag{6}$$

where $n_c = m\omega_0^2/4\pi e^2$ is the critical density. For isothermal conditions, the solution is

$$n(\mathrm{r}) = n_0(\mathrm{r})\exp\left(-\frac{(E_0^2 + E_1^2)_{\rm av}}{8\pi n_c(T_e + T_i/Z)}\right), \tag{7}$$

where $n_0(\vec{r})$ is the static density at low irradiance.

We now assume paraxial ray conditions; i.e., allow the pump (E_0) and acoustic (δn) waves to propagate approximately along the $-z$ direction, while the backscatter (E_1) travels approximately along $+z$. For simplicity, the condition $n_0 = n_0(z)$ will also be assumed. Following Kauffman and Cohen,[34] one can then remove the rapidly oscillating

portions of Eqs. (4) by expanding in terms of the complex wave amplitudes $\mathcal{E}_0$, $\mathcal{E}_1$, and $\delta\tilde{n}$:

$$E_j(\mathbf{r},t)=\tfrac{1}{2}\mathcal{E}_j(\vec{\mathbf{r}},t)\exp\left(i\sigma_j\int^z k_j(z')dz'-i\omega_j t\right)+\text{c.c.}, \tag{8a}$$

$$\delta n(\vec{\mathbf{r}},t)=\tfrac{1}{2}\delta\tilde{n}(\vec{\mathbf{r}},t)\exp\left(-i\int^z k(z')dz'-i\omega t\right)+\text{c.c.}, \tag{8b}$$

where $\sigma_0\equiv-1$, $\sigma_1\equiv+1$, and the carrier frequencies and propagation vectors satisfy the relations

$$\omega\equiv\omega_0-\omega_1, \tag{9a}$$

$$k(z)\equiv k_0(z)+k_1(z)\simeq 2k_0(z), \tag{9b}$$

$$c^2k_j^2(z)=\omega_j^2-4\pi e^2n_0(z)/m. \tag{10}$$

The acoustic amplitude (and thus the backscatter) cannot grow significantly unless $k(z)$ satisfies the resonance condition[35]

$$k(z)\approx k_s=\omega/c_s; \tag{11}$$

i.e., the k-vector mismatch[36]

$$\Delta k(z)\equiv k(z)-k_s \tag{12}$$

should satisfy $|\Delta k(z)|\ll k_s$.

Expressions (8)–(12) are now substituted into Eqs. (4a) and (4b), subject to the restrictions

$$k_0\gg\alpha,\quad K^2/k_0\gg L_k^{-1}, \tag{13}$$

where L_k is the gradient scale lengths of $k(z)$. The equations for the (slowly-varying) steady-state amplitudes then reduce to

$$\left(\frac{\partial}{\partial z}+\frac{i}{2k_0}\nabla_T^2\right)V_0=-\frac{ik_0}{2\epsilon}\frac{n_0-n}{n_c}V_0+\frac{ik_0}{4\epsilon}\frac{\delta\tilde{n}}{n_c}V_1, \tag{14a}$$

$$\left(\frac{\partial}{\partial z}-\frac{i}{2k_1}\nabla_T^2\right)V_1=+\frac{ik_0}{2\epsilon}\frac{n_0-n}{n_c}V_1-\frac{ik_0}{4\epsilon}\frac{\delta\tilde{n}^*}{n_c}V_0, \tag{14b}$$

$$\left(\frac{\Delta\omega_s}{2}+ic_s\Delta k-c_s\frac{\partial}{\partial z}-i\frac{c_s}{2k_s}\nabla_T^2\right)\delta\tilde{n}=\frac{c_s}{8\eta v_e^2}\left(\delta\tilde{n}\frac{\partial}{\partial z}+\frac{i}{k_s}\vec{\nabla}_T\cdot\delta\tilde{n}\vec{\nabla}_T\right)(|V_0|^2+|V_1|^2)-i\frac{k_sc_sn}{4\eta}\frac{V_0V_1^*}{v_e^2}, \tag{14c}$$

where $\vec{\nabla}_T\equiv(\partial/\partial x,\partial/\partial y)$ is the transverse gradient operator, $V_j(\mathbf{r})\equiv e\mathcal{E}_j(\vec{\mathbf{r}})/m\omega_j$ are the electron quiver velocity amplitudes, $v_e\equiv(T_e/m)^{1/2}$ is the electron thermal velocity, $\epsilon\equiv1-n_0/n_c$ is the plasma dielectric constant, and $\eta\equiv1+3T_i/ZT_e$. [On the right-hand sides of Eqs. (14), we have approximated $k_1\simeq k_0=\epsilon^{1/2}\omega_0/c$ and $k\simeq k_s$.] The ∇_T^2 terms in these equations account for diffraction effects, while the (n_0-n) terms describe the intensity-dependent phase shifts and self-focusing. This intensity dependence is given by Eq. (7), which can be written as

$$n(\vec{\mathbf{r}})=n_0(\vec{\mathbf{r}})\exp\left(-\frac{|V_0|^2+|V_1|^2}{4\eta' v_e^2}\right), \tag{15}$$

where $\eta'\equiv1+T_i/ZT_e$.

To evaluate the final terms of Eqs. (14a) and (14b), one must solve (14c) for $\delta\tilde{n}(\vec{\mathbf{r}})$. The present paper will deal only with the strong-damping limit[12,13] where $\Delta\omega_s$ predominates over the convective, diffraction, and phase mismatch terms in (14c); i.e.,

$$\Delta\omega_s/c_s\gg\alpha,\quad K^2/k_0,\quad \Delta k. \tag{16}$$

Then

$$\delta\tilde{n}(\vec{\mathbf{r}})/n(\vec{\mathbf{r}})\simeq-i(Q/2\eta)V_0V_1^*/v_e^2, \tag{17}$$

where $Q\equiv k_sc_s/\Delta\omega_s=\omega/\Delta\omega_s$ can be interpreted as the "quality factor" of the ion-acoustic resonance. Condition (16) is most likely to be found in the low density corona region where ion Landau damping is heavy,[12] and the plasma scale lengths are large.[10] The effects of the phase mismatch[36] on optical ray retracing will be examined in a later publication.

Substituting expression (17) into Eqs. (14a) and (14b), one finally obtains

$$\left(\frac{\partial}{\partial z}+\frac{i}{2k_0}\nabla_T^2\right)V_0=-\frac{ik_0}{2\epsilon}\frac{n_0-n}{n_c}V_0+\frac{k_0Q}{8\epsilon\eta}\frac{n}{n_c}\frac{|V_1|^2}{v_e^2}V_0, \tag{18a}$$

$$\left(\frac{\partial}{\partial z}-\frac{i}{2k_1}\nabla_T^2\right)V_1=+\frac{ik_0}{2\epsilon}\frac{n_0-n}{n_c}V_1+\frac{k_0Q}{8\epsilon\eta}\frac{n}{n_c}\frac{|V_0|^2}{v_e^2}V_1. \tag{18b}$$

The final terms of (18a) and (18b) describe the pump depletion and gain, respectively. Except for these (and the small difference between k_1 and k_0), the equations for V_1 and V_0^* would be identical. This is the reason why the backscatter field amplitude $\mathcal{E}_1=(m/e)\omega_1V_1$ can become proportional to the conjugate pump amplitude $\mathcal{E}_0^*=(m/e)\omega_0V_0^*$ when the gain term is small in comparison to the diffraction.[1]

In solving Eqs. (18), some care must be taken to insure that the condition $|\delta\tilde{n}|\ll n$ remains satisfied; i.e., according to expression (17), the formalism cannot simultaneously treat heavy pump depletion ($|V_1|\approx|V_0|$) *and* large static ponderomotive density variations ($|V_0|^2\approx4v_e^2$). The calculations presented in this paper will ignore pump depletion entirely, and thus assume $|V_1|\ll|V_0|$. Since most of the examples chosen here will also satisfy the condition $|V_0|^2\ll4v_e^2$, it is instructive to write Eqs. (18) with these approximations:

$$\left(\frac{\partial}{\partial z}+\frac{i}{2k_0}\nabla_T^2\right)V_0 \simeq -\frac{i}{\eta'}\frac{k_0}{8\epsilon}\frac{n_0}{n_c}\frac{|V_0|^2}{v_e^2}V_0, \quad (19a)$$

$$\left(\frac{\partial}{\partial z}-\frac{i}{2k_1}\nabla_T^2\right)V_1 \simeq \left(\frac{i}{\eta'}+\frac{Q}{\eta}\right)\frac{k_0}{8\epsilon}\frac{n_0}{n_c}\frac{|V_0|^2}{v_e^2}V_1. \quad (19b)$$

From (19b), one then sees that the ratio of the gain to self-focusing terms becomes $(\eta'/\eta)Q \approx Q \gtrsim 1$, as noted in Sec. I and Ref. 30.

A complete solution of Eqs. (18) or (19) would require an absorption and hydrodynamic model that relates $n_0(\vec{r})$, $T_e(\vec{r})$, and $Q(\vec{r})$ to the incident irradiance, and would include self-consistent ion heating[12] and various ion wave saturation mechanisms.[5,15-17] Initially, however, we wish to concentrate on the role played by diffraction and self-focusing in the ray retracing. The examples presented here will therefore deal with the simplest model where n_0, T_e, and Q are either constants or predetermined functions of position. The inclusion of a self-consistent hydrodynamic model or ion wave saturation must be reserved for a later study.

III. PROPAGATION CODE

In its present form, BOUNCE solves Eqs. (18) [ignoring the $|V_1|^2/v_e^2$ term in (18a)] in two Cartesian coordinates (x,z), using a fast Fourier transform subroutine[37] to handle the transverse (x) variation. If $\tilde{V}_j(\kappa,z)$ is the Fourier transform of $V_j(x,z)$; i.e.,

$$\tilde{V}_j(\kappa,z)=\tilde{T}(V_j(x,z)), \quad V_j(x,z)=\tilde{T}^{-1}(\tilde{V}_j(\kappa,z)), \quad (20)$$

then Eqs. (18) become

$$\left(\frac{\partial}{\partial z}-\frac{i\kappa^2}{2k_0}\right)\tilde{V}_0=-\tilde{T}\left(\frac{ik_0}{2\epsilon}\frac{n_0-n}{n_c}V_0\right), \quad (21a)$$

$$\left(\frac{\partial}{\partial z}+\frac{i\kappa^2}{2k_1}\right)\tilde{V}_1=\tilde{T}\left(\frac{ik_0}{2\epsilon}\frac{n_0-n}{n_c}V_1+\frac{k_0Q}{8\epsilon\eta}\frac{n}{n_c}\frac{|V_0|^2}{v_e^2}V_1\right), \quad (21b)$$

where n is given by Eq. (15).

As we have shown, the wavefront reversal is most effective when the diffraction term $\kappa^2/2k_j$ is large in comparison to the gain and self-focusing terms. This rapidly varying part can be effectively removed from the integration by using the unitary transformations

$$\tilde{V}_j(\kappa,z)\equiv\tilde{V}_j'(\kappa,z)\exp(-i\sigma_j\kappa^2 z/2k_j), \quad (22)$$

(where $\sigma_0=-1$ and $\sigma_1=+1$) to rewrite (21a) and (21b) in the "interaction representation"

$$\frac{\partial\tilde{V}_0'}{\partial z}=-\exp\left(-\frac{i\kappa^2 z}{2k_0}\right)\tilde{T}\left(\frac{ik_0}{2\epsilon}\frac{n_0-n}{n_c}V_0\right), \quad (23a)$$

$$\frac{\partial\tilde{V}_1'}{\partial z}=\exp\left(\frac{i\kappa^2 z}{2k_1}\right)\tilde{T}\left(\frac{ik_0}{2\epsilon}\frac{n_0-n}{n_c}V_1+\frac{k_0Q}{8\epsilon\eta}\frac{z}{n_c}\frac{|V_0|^2}{v_e^2}V_1\right). \quad (23b)$$

These equations are then integrated by a predictor-corrector technique, using Eqs. (20) and (22) to obtain $V_0(x,z)$ and $V_1(x,z)$ at each new point along z.

The input parameters include the density $n_0(z)$, quality factor Q, temperature ratio T_i/T_e, wavelengths λ_j, and incident optical field amplitudes $\mathcal{E}_j(\vec{r})=(m\omega_j/e)V_j(\vec{r})$ (see Fig. 3). In all cases treated here, we have chosen $\lambda_0=\lambda_1=1.064$ μm, and for simplicity, have approximated $\epsilon=1$ and $\eta=\eta'=1$. The pump field, whose transverse profile is usually defined at the lens plane, is normalized to a specified average ratio $\langle|V_0|^2\rangle_{z2}/v_e^2$ at the backscatter exit plane $z2$ of the active medium. The average of any quantity $\psi_j(x,z)$ related to the amplitude $V_j(x,z)$ is defined as

$$\langle\psi_j\rangle_z\equiv\int\psi_j(x,z)|V_j(x,z)|^2dx\Big/\int|V_j(x,z)|^2dx, \quad (24)$$

and the axial position z is measured from the focal plane of the lens.

The backscatter "noise" field $\mathcal{E}_1(x,z1)$, which is arbitrarily normalized, is specified at the entrance plane $z1$. Its x dependence was, in most cases, chosen to be a stochastic function with a random phase Gaussian power spectrum of $(1/e)$ angular width $\Delta\theta_1$.[38] For most of the examples discussed here, $\Delta\theta_1=0.25$ rad; however, the backscatter profiles do not depend strongly on $\Delta\theta_1$ for power gains >100.

The code plots the pump and backscatter profiles at the $z1$, $z2$, and lens planes, and calculates several additional parameters. These include the rms widths $2\langle x_j^2\rangle_z^{1/2}$ of the pump and backscatter beams, an effective power gain

$$G\equiv\langle|V_1|^2\rangle_{z2}\langle x_1^2\rangle_{z2}^{1/2}/\langle V_1^2\rangle_{z1}\langle x_1^2\rangle_{z1}^{1/2}, \quad (25)$$

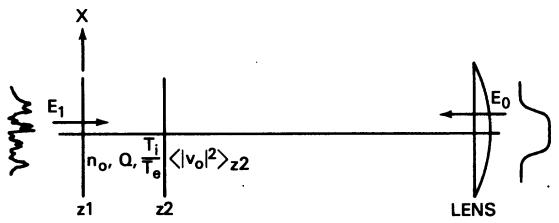

FIG. 3. Input parameters for numerical simulation of Brillouin backscatter from region $z1 \leq z \leq z2$. (The position z is measured from the focal plane of the lens.) The incident pump field $\mathcal{E}_0$ is usually specified at the lens, while the incident noise field $\mathcal{E}_1$ (usually stochastic) is always specified at $z1$.

and an average nonlinear phase shift

$$B \equiv \frac{k_0}{2}\int_{z1}^{z2}\frac{n_0-\langle n\rangle_z}{\epsilon n_c}dz \simeq \frac{k_0}{8\eta'}\int_{z1}^{z2}\frac{n_0}{\epsilon n_c}\frac{\langle|V_0|^2\rangle_z}{v_e^2}dz\,. \tag{26}$$

In most cases, G and B satisfy the approximate relationship $\ln G \approx 2QB$, as one might expect from Eqs. (19). Finally, the code calculates the pump-backscatter correlation function[22,29]

$$H \equiv \left|\int \mathcal{E}_0(x)\mathcal{E}_1(x)dx\right|^2 \Big/ \int|\mathcal{E}_0(x)|^2dx\int|\mathcal{E}_1(x)|^2dx\,, \tag{27}$$

where the field amplitudes are evaluated at the lens. This is a measure of the phase as well as amplitude correlation between the beams, and in the limit of exact wavefront reversal $\mathcal{E}_1(x)\sim\mathcal{E}_0^*(x)$, one obtains $H=1$.

In order to evaluate the accuracy of the code (and provide a graphic illustration of the volume hologram model) we compared it to the analytic theory in a simple test problem. A uniform slab of thickness $L=100$ μm and plasma density $n_0=0.1n_c$ is illuminated directly at $z2=+50$ μm by a pair of intersecting plane waves with hyper-Gaussian profiles; i.e.,

$$\mathcal{E}_0(x,z2)=A(0,x)+A(\theta_D,x)\exp(-ik_0\theta_D x)\,, \tag{28}$$

where $\theta_D=0.16$ rad,

$$A(\theta,x)\sim\exp\{-[2(x-\tfrac{1}{2}L\theta)/d]^{20}\}, \tag{29}$$

and the width d is 180 μm. The resulting interference pattern (Fig. 4) is sufficiently broad and flat that edge effects and gain narrowing[11,29] are unimportant in this case. The quality factor $Q\gg1$ and average intensity $\langle|V_0|^2\rangle_{z2}\ll v_e^2$ were chosen to give an effective (amplitude) gain coefficient $\alpha=0.0376$ μm^{-1} with negligible self-focusing ($B=0$). The backward noise field for this case was a hyper-Gaussian plane wave

$$\mathcal{E}_1(x,z1=-50\ \mu\text{m})=A(\theta_1,x)\exp(+ik_0\theta_1 x) \tag{30}$$

of width 240 μm.

For $\theta_1=0$ (Fig. 4) the backscatter at $z2$ has developed a periodicity *exactly* in phase with that of the pump, as described in Sec. I. This periodicity produces the peaks around $\theta=0$ and 0.16 rad back at the lens plane, as one would expect from Eq. (28). For $\theta_1>0$, the backscatter pattern at $z2$ shifts slightly to the right, thereby reducing the overlap with the pump and lowering the gain.[11] At the lens plane, both peaks shift a distance θ_1 to the right. An analogous shift and lowering of gain occurs when $\theta_1<0$. The resulting tuning curve (Fig. 5) shows good agreement with the analytic theory,[11,24] and illustrates the limitations

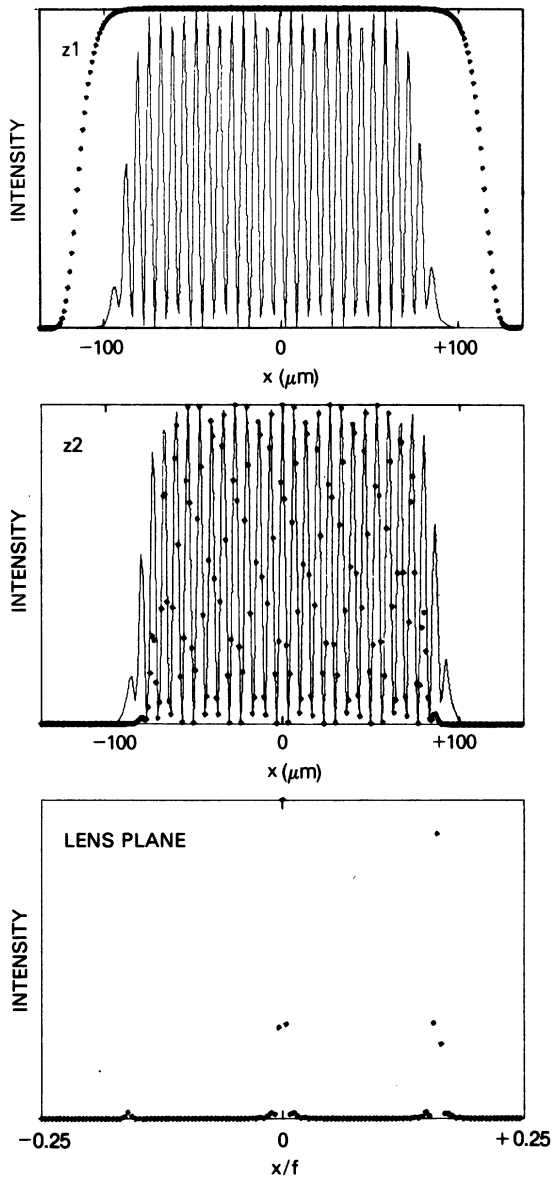

FIG. 4. Transverse intensity profiles for two plane hyper-Gaussian pump waves ($\theta_0\equiv0$, $\theta_0'\equiv\theta_D\equiv0.16$ radian) and a backscatter "noise" wave ($\theta_1=0$) interacting within a uniform 100 μm plasma slab centered at $z=0$. In this and all subsequent profiles, the solid and dotted lines are the normalized pump and backscatter intensities, respectively.

of the volume hologram mechanism. The small discrepancy between the 0.08-rad ($1/e$) width of this curve and the value $\delta\theta\simeq(8/\alpha L)^{1/2}\alpha/k_0\theta_D=0.058$ rad from Eq. (2a) arises from the fact that $\alpha L=3.67$, while (2a) is strictly applicable only if $\alpha L\gg1$.

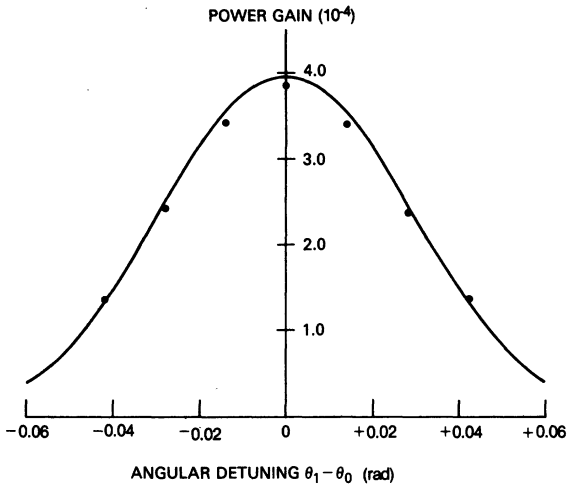

FIG. 5. Tuning curve for the 100 μm slab, showing Brillouin gain G vs angular detuning $\theta_1-\theta_0$. The solid line is the analytic result from Refs. 11 or 24 (exact for infinite plane waves), and the dots are the numerical results from BOUNCE.

IV. RESULTS

In all of the remaining examples, the pump field incident at the lens is assumed to be uniphase. Simulations of wavefront conjugation experiments where the spatial structure of the pump resides in the phase[1-3,20] will be addressed in a later publication.

A. Whole-beam effects

Whole-beam ray retracing is illustrated in Figs. 6–8. In Fig. 6(a), the incident pump profile is a half blocked hyper-Gaussian function of e^{-4} angular width 0.19 rad. This is focused into a 300 μm-thick plasma of exponentially decreasing density[39] $n_0=0.2n_c\exp(-z/l)$, where $l=100$ μm, with the backscatter noise field incident at the focal plane ($z1=0$). To ensure negligible self-focusing in this example, we chose $\langle|V_0|^2\rangle_{z2}\ll v_e^2$, but allowed $Q\gg1$ to obtain a high power gain $\ln G=11$. The long, narrow focal waist within the plasma ($d\approx12$ μm at $z1$ and 70 μm at $z2=300$ μm) amplifies only those noise components traveling back along the pump beam, as seen by comparing the profiles at $z2$ and the lens. The backscatter profile at $z2$ also shows gain narrowing due to higher amplification in the more intense central portion of the pump beam.[18] This also occurs in all subsequent examples, and produces the Gaussian-type tails back at the lens. In spite of such effects, one obtains good field correlation ($H=0.72$), with only 5% of the backscatter hitting the blocked portion of the lens, in qualitative agreement with the experiment of Fig. 1.[10] Similar results are found at higher gain, with somewhat greater broadening at the lens due to more gain narrowing at $z2$.

Conditions in Fig. 6(b) are similar to those in the above example, except that we now choose $Q=1$ and $\langle|V_0|^2\rangle_{z2}/v_e^2=0.104$ to allow significant self focusing ($B=7.6$) along with the high gain $\ln G=8.9$. This is evident in the filamentation of the pump profile at $z1$ and some additional narrowing of the backscatter at $z2$; the backscatter at the lens remains well correlated with the pump ($H=0.70$), with still only 5% in the shadow region.

When the pump field is focused at $z_2=0$, one obtains similar ray retracing behavior, but the self-focusing can cause a pronounced threshold effect.[40] An example of this is shown in Figs. 7(a) and 7(b). A hyper-Gaussian pump field of e^{-4} angular width 0.12 rad is focused to a 20 μm central spot of average intensity $\langle|V_0|^2\rangle_{z2}/v_e^2=0.508$ at $z2$, then propagates through a 400 μm plasma slab of uniform density n_0 and $Q=1$. For $n_0=0.01$ n_c [Fig. 7(a)], the pump beam expands to about 45 μm at $z1$, with self-focusing effects playing only a minor role ($B=1.2$). Although the geometrical conditions are ideal for whole-beam ray retracing, the power gain $\ln G=1.3$ is too low to provide sufficient spatial mode filtering of the broadband noise source; consequently, the effect is minimal.

In Fig. 7(b), the density has been doubled to $n_0=0.02n_c$, increasing the self-focusing ($B=2.9$) and reducing the central beam diameter at $z1$ to about 30 μm. The resulting increase in pump intensity within the slab raises the gain to $\ln G=7.3$, and produces the clear retrace at $z2$ and the lens. The probable reason why $\ln G$ increases faster than B is that after the first one or two e foldings, the backscatter is confined primarily to near-axial backward modes, which are then amplified more effectively in the remaining active material.

Figure 8 illustrates a case where ray retrace would not be expected to occur. Here, the plasma is a uniform slab of density $n_0=0.1n_c$, which lies between 300 and 400 μm. The thickness is smaller than the 180–240 μm (e^{-4}) beam width of the pump, and cannot provide effective filtering action to favor the backward direction. Thus, in spite of high gain $\ln G=7.1$, the ray retrace is minimal, and the backscatter seen at $z2$ is essentially an amplified version of the noise field (whose angular width was broadened to 0.5 rad for this example). Additional evidence for the amplified noise character of the scattered radiation is the low correlation $H\simeq0.001$.

B. Small-scale effects

In the following examples, the pump angular intensity distribution at the lens consists of three

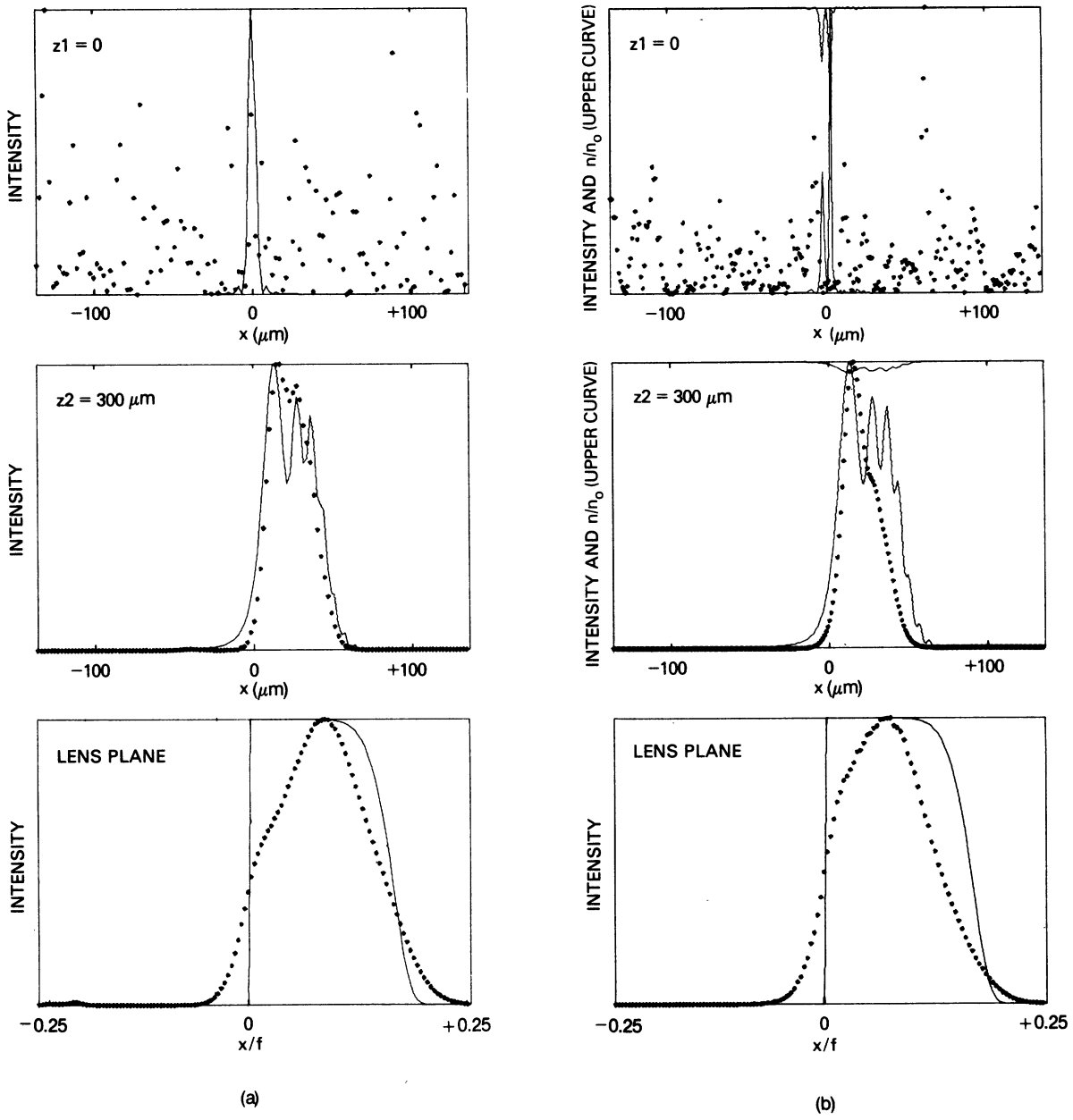

FIG. 6. Transverse profiles of the pump radiation and backscatter from a 300 μm plasma of density $0.2n_c\exp(-z/100)$, showing partial retracing of a half-blocked pump beam at the lens. The stochastic noise appears as random dots at the focal plane $z1=0$. (a) Negligible self-focusing ($B=0$), with $\ln G=11$. (b) Strong self-focusing ($B=7.6$) with comparable gain $\ln G=8.9$. The density variations n/n_0 are given by Eq. (15).

isolated Gaussian peaks of e^{-4} width $\Delta_B/f=0.025$ rad, with the maxima at -0.0664, and 0.0117 and 0.121 rad. The nearest neighbor spacing is thus 0.078 rad, while the total angular spread is 0.187 rad.

In Fig. 9, the pump radiation is focused into a uniform 100 μm slab of plasma density $n_0=0.1n_c$, with a quality factor $Q\gg 1$ and average intensity $\langle|V_0|^2\rangle_{z2}\ll v_e^2$ chosen to produce high gain $\ln G=12.5$ but negligible self-focusing ($B=0$). The three interfering pump beams at the focal plane $z1=0$ produce a quasi-periodic intensity pattern, which is superimposed upon a Gaussian envelope of total width $d\simeq 2\lambda_0 f/\Delta_B\simeq 85$ μm. At the $z2$ plane, this envelope has expanded and shifted somewhat due to the small divergence and separation of the focal waists. Near the axis, where the average gain is high, the backscatter has begun to develop

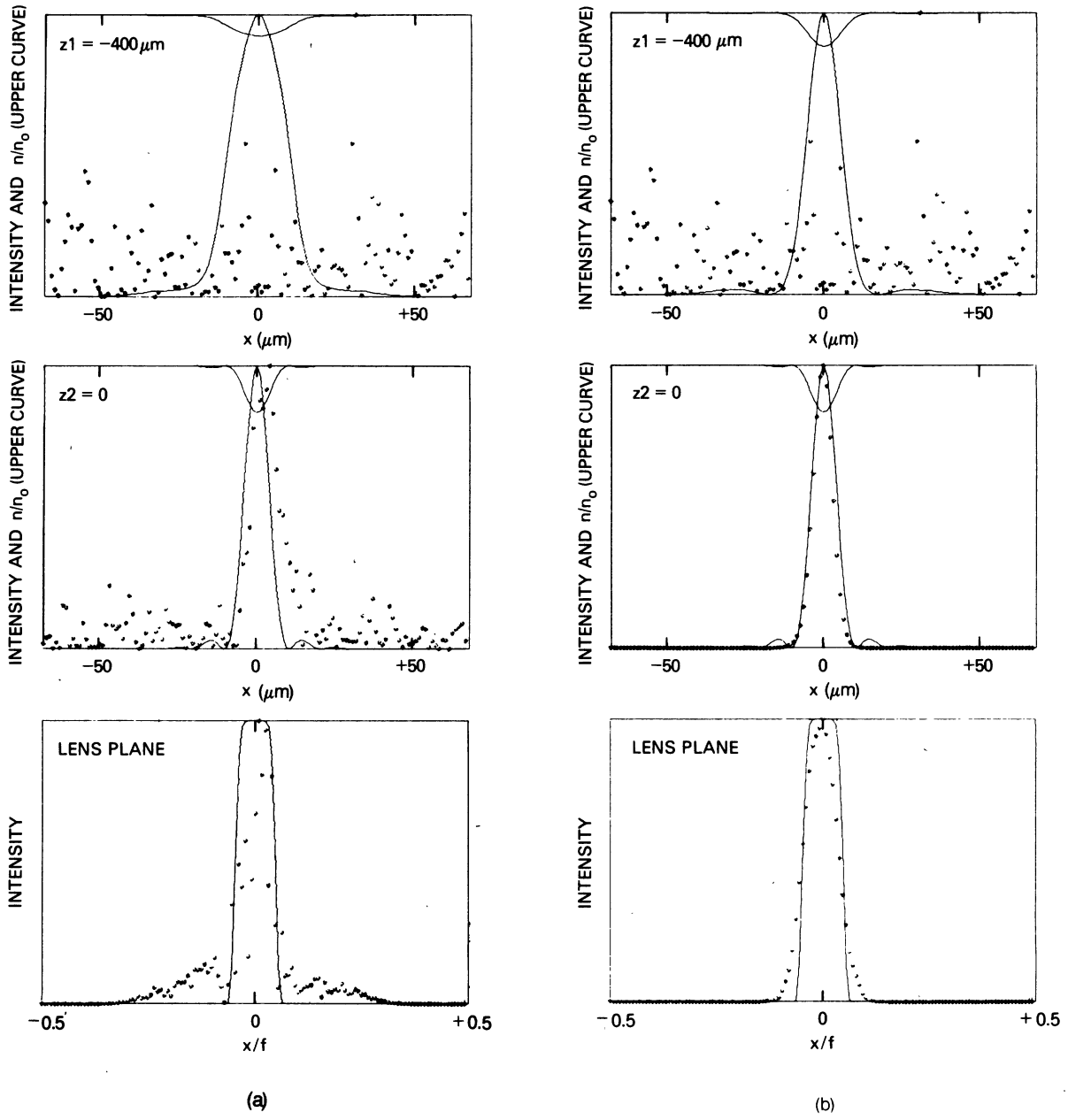

FIG. 7. Transverse profiles for a uniform 400 μm plasma located just beyond the focal plane $z2=0$. (a) Below threshold for retrace ($B=1.2$, $\ln G=1.3$) with $n_0=0.01n_c$. (b) Above threshold ($B=2.9$, $\ln G=7.3$) with the same incident pump intensity, but $n_0=0.02n_c$.

an intensity pattern in phase with that of the pump, just as it did in the test problem (Fig. 4). In this case, however, the spatial gain narrowing[11,29] of the backscatter envelope is more severe, giving a total envelope width of only $d_1 \simeq 30$ μm.

The ray retracing is readily apparent back at the lens plane, but the maxima are slightly displaced, and three additional peaks of significant height are also present. This type of degradation occurs because the angular bandpass of the gain medium (due to its finite thickness) is too broad to effectively filter out all of the nonretracing components in the incident noise spectrum. Using Eq. (2a) with the average amplitude gain coefficient $\alpha \simeq (\frac{1}{8}k_0)(n_0/n_c)Q\langle|V_0|^2\rangle_{z2}/v_e^2 = 0.0524\ \mu\text{m}^{-1}$, one obtains $(\theta_D)_{\min} \simeq 0.1$ rad, which is comparable to the

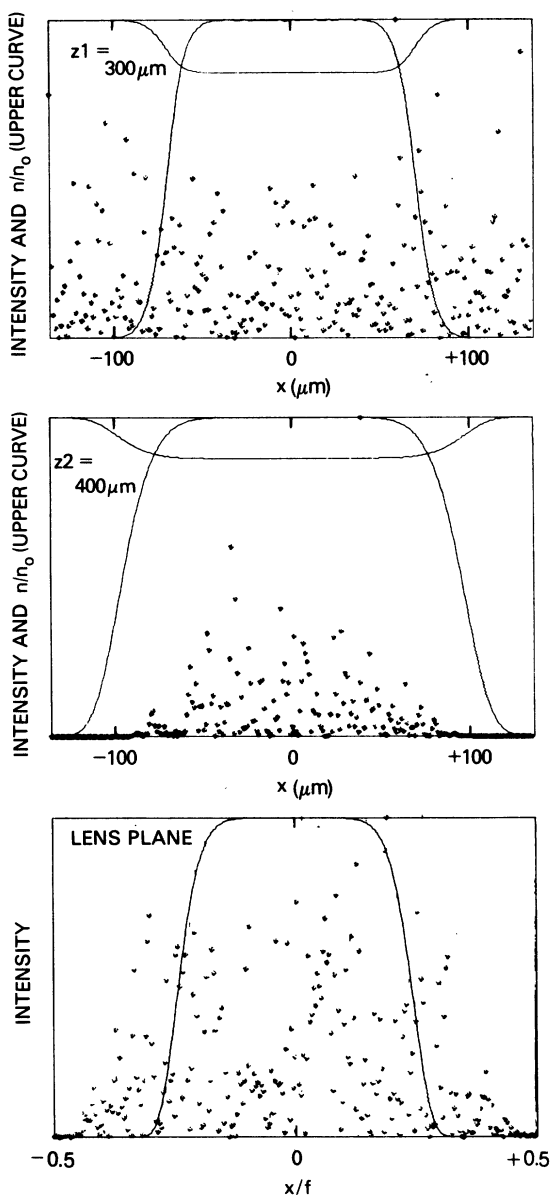

FIG. 8. Transverse profiles for a uniform 100 μm plasma in the quasi-near field of the lens. The whole-beam ray retracing is ineffective when the width of the gain region becomes comparable to its length.

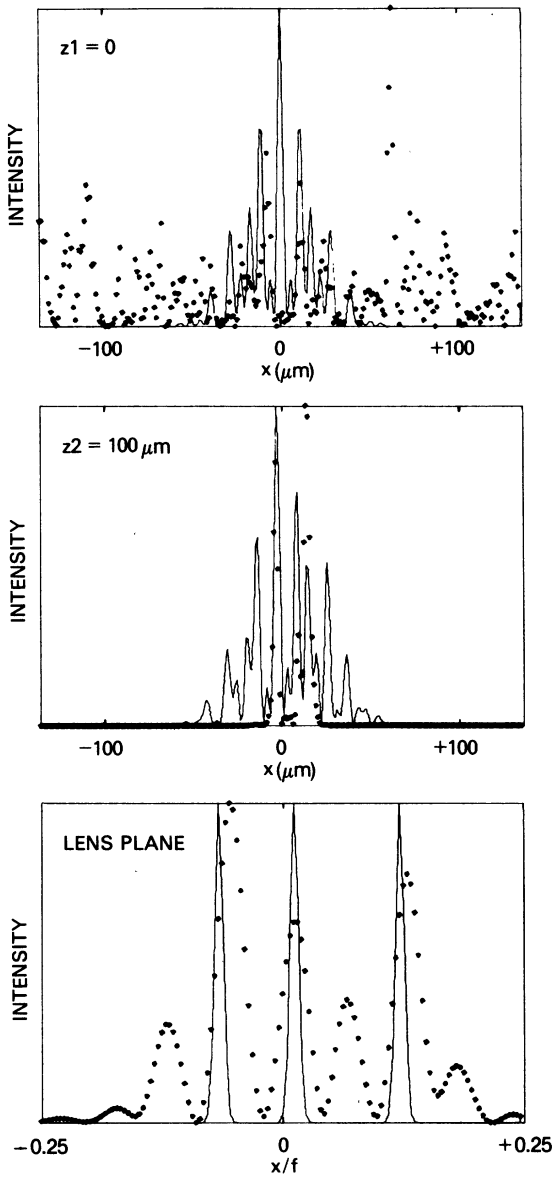

FIG. 9. Transverse profiles for a uniform 100 μm plasma at the focal plane $z1=0$, showing partial retracing of the three pump beams at the lens. ($B=0$, $\ln G = 12.5$.)

angular distance between adjacent peaks in the pump beam. The broadening of the backscatter peaks arises from the gain narrowing[11] noted in the preceding paragraph; i.e., for an envelope of width $d_1 \simeq 30$ μm at $z2$, one obtains a total angular width $2\lambda_0/d_1 \simeq 0.07$ rad back at the lens. The gain narrowing filters out most of the higher spatial frequency structure (from the incident noise) that would otherwise get to the lens plane within the finite angular bandpass of the gain medium.

Figure 10(a) illustrates an enhancement of ray retracing when the uniform slab geometry is replaced by a density gradient of equal scale length and total thickness 300 μm; i.e., $n_0 = 0.2 n_c \exp(-z/l)$, where $l = 100$ μm, and $0 \leq z \leq 300$ μm. We again choose $Q \gg 1$ and $\langle |V_0|^2 \rangle_{z2}/v_e^2 \ll 1$ to obtain $\ln G = 9.2$ with negligible self-focusing ($B=0$). For this case, one can apply Eq. (2b) to estimate $(\theta_D)_{\min} \simeq 0.063$ rad, which should allow the three peaks to be fully resolved in the backscatter. This

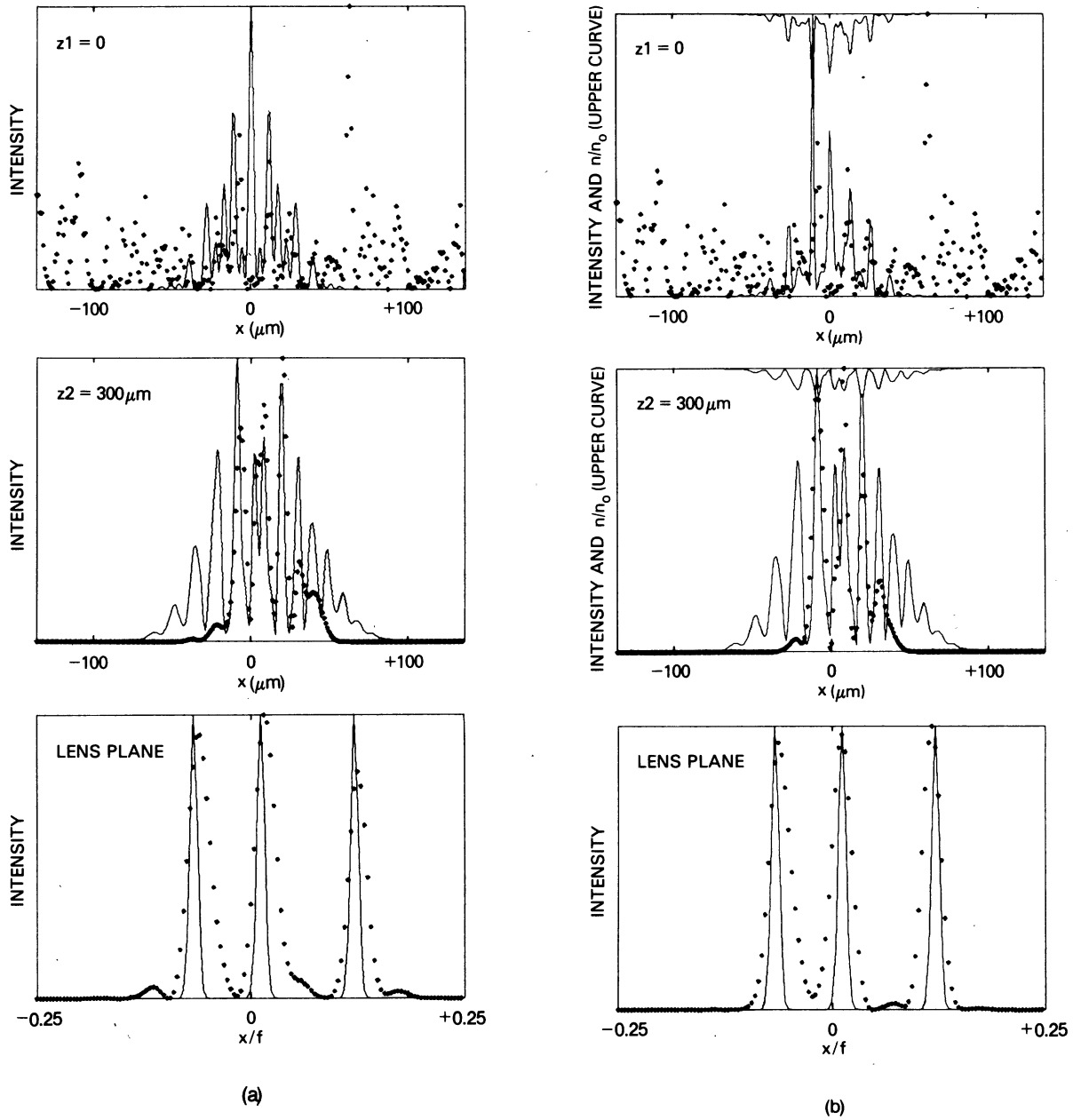

FIG. 10. Transverse profiles for a 300 μm plasma of density $0.2n_c\exp(-z/100)$, showing nearly complete retrace of the three pump beams at the lens. (a) Negligible self-focusing ($B=0$) with $\ln G=9.2$. (b) Strong self-focusing ($B=5.6$) with $\ln G=10$.

expectation is confirmed by the profiles in the lens plane. The three amplitudes are now nearly equal, and the mismatch and additional structure evident in Fig. 9 have almost completely disappeared. An improvement in ray retracing is also evident in the better pump-backscatter synchronization at $z2$, and the larger correlation number $H=0.50$, compared to $H=0.33$ for the preceding case.

The physical reason for such enhancement is that although the plasma beyond 100 μm accounts for only a few e foldings of amplification, the local gain coefficient satisfies condition (3), so the region can still provide significant transverse mode discrimination. For example, the highest (amplitude) gain coefficient in the last two e foldings of intensity (the region between 135 and 300 μm) is 0.013 μm^{-1}, giving a $1/e$ gain length of 77 μm. From the known angular separations at the lens, one obtains $K_{min}/k_0=0.078$ rad, giving a maximum diffraction length of $k_0/K_{min}^2=28$ μm.

A comparison between the $z2$ profiles in Figs. 9 and 10(a) reveals that gain narrowing is less evident in the gradient geometry, presumably because of a greater opportunity for diffraction spreading in the 100–300 μm region. This results in slightly narrower backscatter peaks at the lens; however, the residual broadening is still evident, and it appears to be the primary reason why $H<1$. A similar reduction of wavefront reversal due to spatial gain narrowing was predicted in Ref. 29.

In Fig. 10(b), the conditions are similar to those of Fig. 10(a), except that we now choose $Q=1$ and $\langle|V_0|^2\rangle_{z2}/v_e^2=0.213$ to allow self-focusing ($B=5.6$) along with the high gain $\ln G=10.0$. This causes some filamentation and shifting of the pump intensity spikes at $z1$, but little narrowing of the envelope. The effect on the backscatter profile at $z2$ is minimal. Except for small differences in the amplitude of the spikes and a slight envelope narrowing, this intensity distribution is essentially the same as that of Fig. 10(a). Back at the lens, the ray retrace appears to have actually been enhanced somewhat, and the correlation has increased to $H=0.55$.

The relatively minor influence of self-focusing in this example can be qualitatively understood in terms of Bespalov-Talanov perturbation theory.[41] According to this theory, a small intensity ripple of spatial frequency κ grows exponentially at the rate

$$\alpha_{SF}=\left(\frac{1}{k_0}\frac{dB}{dz}-\frac{\kappa^2}{4k_0^2}\right)^{1/2}\cdot\kappa \tag{31}$$

due to self-focusing effects. If κ exceeds the cutoff frequency $\kappa_c=(4k_0dB/dz)^{1/2}$, then α_{SF} becomes imaginary and the growth ceases; i.e., the diffraction spreading begins to outweigh the nonlinearity. For the spatial frequencies in the interference pattern, this condition prevails over almost all of the 125–300 μm region in which the last two Brillouin e foldings (and hence significant backscatter profile modifications) are taking place. The small decrease in widths of the pump envelope at $z1$ [$d_0(B=5.6)=82$ μm, compared to $d_0(B=0)=85$ μm from Fig. 10(a)], and the backscatter at $z2$ [$d_1(B=5.6)=75$ μm, compared to $d_1(B=0)=80$ μm from Fig. 10(a)] shows that whole-beam self-focusing is relatively unimportant in this example. However, at the low spatial frequencies corresponding to such widths, expression (31) gives $\alpha_{SF}\sim\kappa\sim 1/d_j$. One should therefore expect whole-beam effects to appear if either $d_0(B=0)$ or $d_1(B=0)$ become significantly smaller. This point is illustrated in the next set of examples.

Conditions in Fig. 11(a) are similar to those in Fig. 10(a), except that the pump beams are now focused at $z2$ rather than $z1$. With $B=0$ and $\ln G=12$, this configuration retraces as well as the earlier examples, and gives a correlation $H=0.52$. The total width of the backscatter envelope at $z2$ is now only 60 μm, however, and a deterioration of the retrace due to whole-beam self-focusing soon becomes apparent as B increases. For $B=2.77$ and $\ln G=12$ ($Q=2$), the middle peak decreases by 25%, and the one on the right by 50%. For $B=5.17$ and $\ln G=9.4$ ($Q=1$), the retracing has almost completely disappeared, as seen in Fig. 11(b), and the correlation has dropped to $H=0.107$. The whole-beam self-focusing responsible for this is clearly evident at the $z2$ plane.

Finally, Fig. 12 illustrates the importance of the holographic mechanism in small scale ray retracing. Here, the inhomogeneous plasma lies between $z1=900$ μm and $z2=1200$ μm, so that the pump beams remain almost completely separated from one another. Each one therefore generates its own whole-beam backscatter from the random noise field in its vicinity, as seen at the $z2$ plane. Since these backscatter amplitudes are more or less random, and their phases remain uncorrelated, they will combine to produce only random patterns back at the lens.

V. SUMMARY AND CONCLUSIONS

In this paper, we have performed numerical studies of optical ray retracing in stimulated backscatter from laser-produced plasmas. Ray retracing was found to be influenced by several factors, such as the optical diffraction lengths, gain inhomogeneity, gain narrowing, self-focusing, and the size and location of the focal spot.

For whole-beam retracing, which arises from the high axial gain within a long, narrow focal waist, we found the following results: (i) In simulations where a half-blocked beam is focused near the critical surface of an inhomogeneous plasma, only a small portion (5%) of the backscatter returns to the lens in the shadow region. This demonstrates that the reflection is nonspecular, and is in good qualitative agreement with a recent Naval Research Laboratory (NRL) experiment.[10] (ii) Because of gain narrowing effects within the focal waist, the spatial profile of the backscatter at the lens tends to have broader wings than that of the pump beam. (iii) The backscatter profile at the lens is relatively insensitive to self-focusing, provided that the Brillouin gain is sufficiently high (e.g., $G>100$). At lower gain, self-focusing can cause the retracing to exhibit a pronounced threshold with respect to variations of density or pump irradiance, especially when the plasma is placed just beyond the focal plane. (iv) When the target is moved far out of focus, so that the beam width

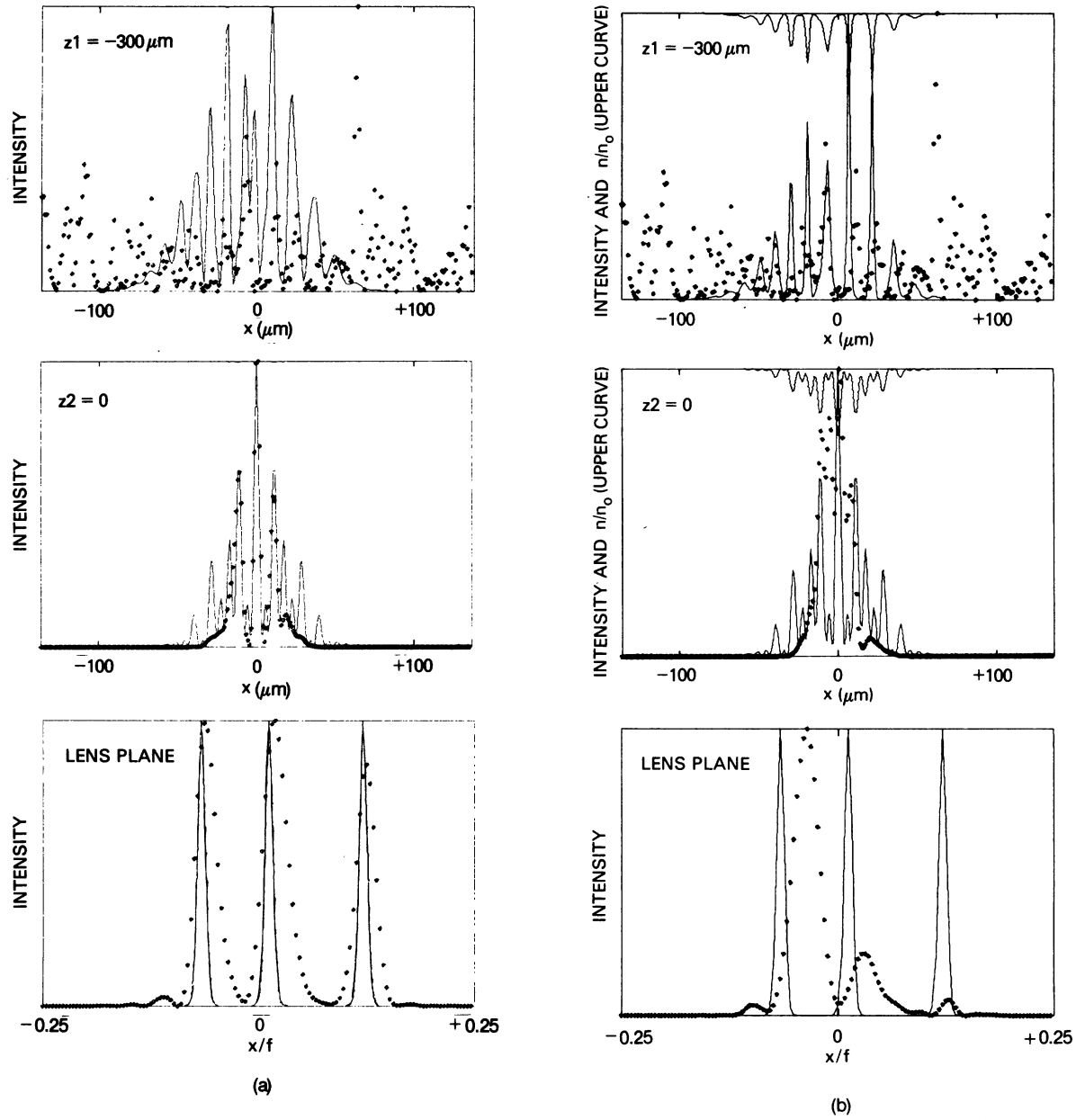

FIG. 11. Transverse profiles for a 300 μm plasma of density $0.2n_c \exp[-(z+300)/100]$, showing the degradation of small scale retrace by whole-beam self-focusing. (a) Negligible self-focusing ($B=0$) with $\ln G = 12$. (b) Strong self-focusing ($B=5.17$) with $\ln G = 9.4$.

becomes comparable to the length of the gain region, the retrace effect disappears, and the backscatter profile becomes essentially that of amplified noise.

Small-scale retracing or wavefront reversal occurs when the transverse structure of the pump beam creates a broad interference pattern in the plasma, which then behaves as an active volume hologram. According to this model, effective wavefront reversal requires that the gain occur slowly over typical diffraction lengths $1/k_0\theta_D^2$. Excellent agreement was found between a simple coupled wave analysis of the model,[11,24] and the numerical solutions of an idealized test problem where two truncated plane waves formed an interference pattern in a uniform plasma.

In more realistic simulations, we chose a pump profile consisting of three isolated hot spots at the

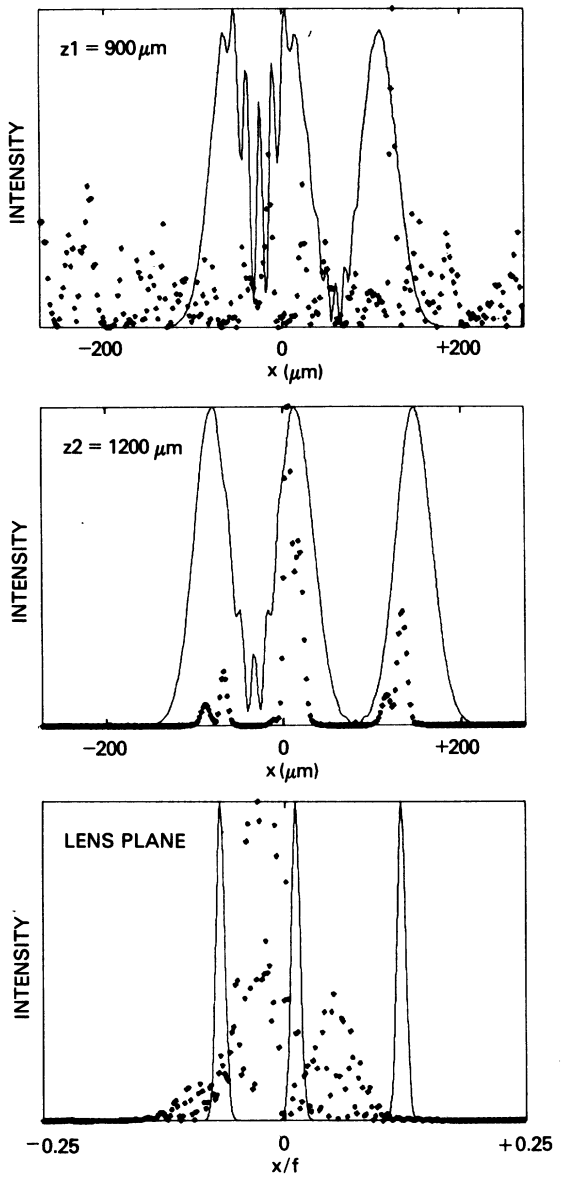

FIG. 12. Transverse profiles for a 300 μm plasma of density $0.2n_c \exp[-(z-900)/100]$, illustrating that small-scale retrace disappears when the pump beams do not overlap.

lens, producing an interference pattern of ≈100 μm width near focus. These simulations produced the following results: (i) Wavefront reversal is enhanced if the plasma has a monotonically decreasing gain coefficient away from the target. For example, a plasma density variation $\exp(-z/l)$, where $l \gg 1/k_0\theta_D^2$, produces significantly better wavefront reversal than a uniform slab of thickness l and comparable net gain. This enhancement arises from the better spatial filtering action that occurs in the lower gain region $z > l$. (ii) Gain narrowing effects, which were present in all cases, restrict the number of periods within the backscatter interference pattern.[11,29] At the lens plane, this tends to eliminate higher spatial frequencies and broaden the hot spots in the backscatter. (iii) In the case of a plasma density $\sim\exp(-z/l)$, self-focusing appears to have a minimal effect on the wavefront reversal, provided that $l \gg 1/k_0\theta_D^2$ and the width of the backscatter interference pattern is large in comparison to its period. If this width decreases below a critical value, then whole-beam self-focusing takes over and destroys the wavefront reversal. This is especially likely in cases where gain narrowing effects are prominent, or where the pump beams are focused a few hundred microns in front of the target. (iv) If the target is moved into the quasi-near field of the lens, so that the hot spots no longer interfere, the wavefront reversal disappears, and the backscatter profile assumes a random noise character. The formation of a volume hologram is therefore essential for wavefront reversal.

So far, this work has been restricted to the strong damping limit, and pump depletion has been ignored. In a future study, we will attempt to incorporate phase mismatch, pump depletion, self-consistent ion heating and ion wave saturation into the code, and to simulate actual phase-conjugation experiments. As suggested in Refs. 11 and 29, effects such as pump depletion and ion wave heating are likely to improve the ray retracing by reducing spatial gain narrowing.

ACKNOWLEDGMENTS

The authors wish to thank Stephen Bodner, John McMahon, Barrett Ripin, and Kenneth Whitney for their encouragement and valuable discussions. This work was supported by the U. S. Department of Energy.

[1]B. Ya. Zel'dovich, V. I. Popovichev, V. V. Ragul'skii, and F. S. Faizullov, Pis'ma Zh. Eksp. Teor. Fiz. 15, 160 (1972) [JETP Lett. 15, 109 (1972)].

[2]V. N. Blashchuk *et al.*, Pis'ma Zh. Tekh. Fiz. 3, 211 (1977) [Sov. Tech. Phys. Lett. 3, 83 (1977)]; V. Wang and C. R. Guiliano, Opt. Lett. 2, 4 (1978); R. Mays, Jr. and R. J. Lysiak, Optics Commun. 31, 89 (1978).

[3]O. Yu. Nosach, V. I. Popovichev, V. V. Ragul'skii, and

F. S. Faizullov, Pis'ma Eksp. Teor. Fiz. 16, 617 (1972) [JETP Lett. 16, 435 (1972)]; B. N. Borisov, Yu. I. Kruzhilin, and S. V. Shklyarik, Pis'ma Zh. Tekh. Fiz. 4, 160 (1978) [Sov. Tech. Phys. Lett. 4, 66 (1978)]; N. F. Pilepetskii, V. I. Popovichev, and V. V. Ragul'skii, Pis'ma Zh. Eksp. Teor. Fiz. 27, 619 (1978) [JETP Lett. 27, 585 (1978)]; N. G. Basov *et al.*, Kvant. Elektron. (Moscow) 6, 765 (1979) [Sov. J. Quantum Electron. 9, 455 (1979)].

[4]V. I. Bespalov, A. A. Betin, and G. A. Pasmanik, Pis'ma Zh. Tekh. Fiz. 3, 215 (1977) [Sov. Tech. Phys. Lett. 3, 85 (1977)].

[5]M. J. Herbst, C. E. Clayton, and F. F. Chen, Phys. Rev. Lett. 43, 1591 (1979).

[6]J. C. Samson, H. A. Baldis, N. H. Burnett, and P. B. Corkum, Eighth Annual Conference on Anomalous Absorption of Electromagnetic Waves, (unpublished).

[7]K. Eidmann and R. Sigel, in *Laser Interaction and Related Plasma Phenomena*, edited by H. J. Schwarz and Heinrich Hora (Plenum, New York, 1974), Vol. 3B.

[8]J. A. Stamper *et al.*, Ref. 7.

[9]N. G. Basov *et al.*, Kvant. Elektron. 4, 2268 (1977) [Sov. J. Quantum Electron. 7, 1300 (1977)].

[10]B. H. Ripin, F. C. Young, J. A. Stamper, C. M. Armstrong, R. Decoste, E. A. McLean, and S. E. Bodner, Phys. Rev. Lett. 39, 611 (1977); B. H. Ripin, Naval Research Laboratory Memorandum Report No. 3684, 1977 (unpublished).

[11]R. H. Lehmberg and B. H. Ripin, *Proceedings of the International Conference on Lasers '78*, edited by V. J. Corcoran (STS, McLean, Va., 1979).

[12]D. W. Phillion, W. L. Kruer, and V. C. Rupert, Phys. Rev. Lett. 39, 1529 (1977).

[13]C. L. Tang, J. Appl. Phys. 37, 2945 (1966).

[14]P. Kaw, G. Schmidt, and T. Wilcox, Phys. Fluids 16, 1522 (1973).

[15]W. L. Kruer, Phys. Fluids 23, 1273 (1980); J. M. Dawson, W. L. Kruer, and B. Rosen, *Dynamics of Ionized Gases*, edited by M. Lighthill, I. Imai, and H. Sato (University of Tokyo Press, Tokyo, 1973), p. 47.

[16]A. Ng, L. Pitt, D. Salzmann, and A. A. Offenberger, Phys. Rev. Lett. 42, 307 (1979).

[17]D. W. Forslund, J. M. Kindel, and E. L. Lindman, Phys. Fluids 18, 1002 (1975); 18, 1017 (1975).

[18]H. Kogelnik, Appl. Opt. 4, 1562 (1965); D. Cotter, D. C. Hanna, and R. Wyatt, Appl. Phys. 8, 333 (1975).

[19]A. I. Sokolovskyaya, G. L. Brekhovskiskii, and A. D. Kudryautseva, Opt. Commun. 24, 74 (1978).

[20]B. Ya. Zel'dovich, N. A. Mel'nikov, N. F. Pilipetskii, and V. V. Ragul'skii, Pis'ma Zh. Eksp. Teor. Fiz. 25, 41 (1977) [JETP Lett. 25, 36 (1977)].

[21]V. G. Sidorovich, Zh. Tekh. Fiz. 46, 2168 (1976) [Sov. Phys. Tech. Phys. 21, 1270 (1976)].

[22]B. Ya. Zel'dovich and V. V. Shkunov, Kvant. Electron. 5, 36 (1978) [Sov. J. Quantum Electron. 8, 15 (1978)]; 4, 1090 (1977) [7, 610 (1977)].

[23]R. W. Hellwarth, J. Opt. Soc. Am. 68, 1050 (1978).

[24]R. H. Lehmberg, Phys. Rev. Lett. 41, 863 (1978).

[25]V. V. Ragul'skii, Tr. Fiz. Inst. Akad. Nauk SSSR 85, 3 (1976); E. G. Kochemasov and V. D. Nikolaev, Kvant. Elektron. 4, 115 (1977) [Sov. J. Quantum Elektron. 7, 60 (1977)].

[26]I. M. Bel'dyugin, M. G. Galushkin, E. M. Zemskov, and V. I. Mandrosov, Kvant. Elektron. 3, 2467 (1976) [Sov. J. Quantum Electron. 6, 1349 (1976)].

[27]H. Kogelnik, Bell Syst. Tech. J. 48, 2909 (1969).

[28]The possibility of producing a similar effect in a resonantly pumped laser medium has recently been examined by A. N. Oraevskii, Kvant. Elektron. 6, 218 (1979) [Sov. J. Quantum Electron. 9, 119 (1979)].

[29]N. B. Baranova, B. Ya. Zel'dovich, and V. V. Shkunov, Kvant. Elektron. 5, 973 (1978) [Sov. J. Quantum Electron. 8, 559 (1978)].

[30]B. I. Cohen and C. E. Max, Phys. Fluids. 22, 1115 (1979).

[31]B. Langdon and B. F. Lasinski, Phys. Rev. Lett. 34, 935 (1975).

[32]W. L. Kruer, 20th Scottish University Summer School in Physics, St. Andrews, Scotland, 1979, Lawrence Livermore Laboratory Report No. UCRL-83149 (unpublished), p. 31.

[33]C. S. Liu, *Advances in Plasma Physics*, edited by A. Simon and W. B. Thompson (Wiley, New York, 1976), Vol. 6, p. 121.

[34]A. N. Kaufman and B. I. Cohen, Phys. Rev. Lett. 30, 1306 (1973).

[35]These results are applicable only if the plasma blowoff velocity $\vec{u}$ satisifies the condition $|\vec{u}| \ll c_s$. More generally, the operators $\partial/\partial t$ and $\partial^2/\partial t^2$ in Eq. (4b) would be replaced by the convective derivatives $\partial/\partial t + \vec{u}\cdot\vec{\nabla}$ and $(\partial/dt + \vec{u}\cdot\vec{\nabla})^2$, respectively, and Eq. (11) would be replaced by $k_s = \omega/(c_s - u_x)$.

[36]C. S. Liu, M. N. Rosenbluth, and R. B. White, Phys. Fluids 17, 1211 (1974).

[37]E. O. Brigham, *The Fast Fourier Transform* (Prentice-Hall, Englewood Cliffs, 1974).

[38]Even if the net Brillouin gain is low, the introduction of a noise source at $z1$ (rather than a volume distribution, as in Ref. 29) is justified here because most of the noise is likely to arise from diffuse reflection near the critical surface [e.g., see C. J. Randall, J. J. Thompson, and K. G. Estabrook, Phys. Rev. Lett. 43, 924 (1979)].

[39]Experiments performed at the Naval Research Laboratory (Ref. 10) indicate that most of the Brillouin gain occurs in the low-density corona region beyond $\sim 0.1\eta_c$.

[40]W. Kaiser and M. Maier, *Laser Handbook*, edited by F. T. Arecchi and E. O. Schulz-Dubois (North-Holland, Amsterdam, 1972), Vol. 2.

[41]V. I. Bespalov and V. I. Talanov, Pis'ma Zh. Eksp. Teor. Fiz. 3, 471 (1966) [JETP Lett. 3, 307 (1966)].

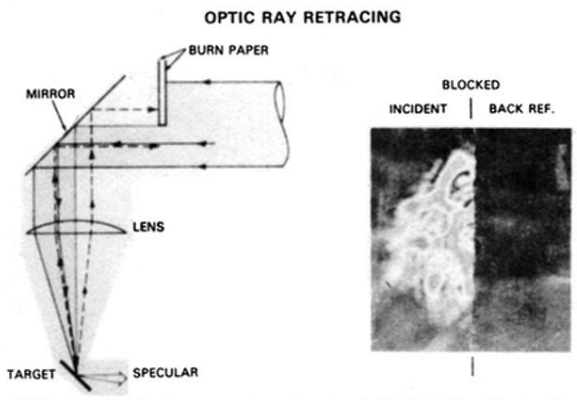

FIG. 1. Optical ray retracing test (Ref. 10). No back-reflection exposure is found on the blocked half of the beam, indicating that ray retracing occurs.